Dispersivity of Bidisperse Packings of Spheres and Evidence for Distinct Random Structures

U. M. Scheven*
Department of Biomedical Engineering, University of Michigan, Ann Arbor, Michigan 48109, USA

(Received 21 December 2017; published 18 May 2018)

The intrinsic longitudinal and transverse dispersivity of bidisperse random packings of spheres with size ratio 5:1 was determined by pulsed field gradient nuclear magnetic resonance, in the dilute regime where small spheres occupy between 0% and 5% of the packings' volume. Small spheres plugging pores systematically raise the mechanical transverse and longitudinal dispersivity above that of reference packings of monodisperse spheres. NMR-derived porosities, widths of velocity distributions, and dispersivities reveal distinct states of structural disorder above and below a relative sphere concentration $n/N = 1$, where n and N are the number densities of small and large spheres.

DOI: 10.1103/PhysRevLett.120.208006

The random packing of monodisperse spheres (RPMS) is commonly used to study tracer dispersion by constant Stokes flow and diffusion in disordered porous media. This process is of profound importance in chemical separations, chromatography, and reactors, and in the spread of contaminant plumes in aquifers[1–4]. The conceptual simplicity of the RPMS geometry and the ease with which a packing can be made in the laboratory or prepared "*in silico*" enable robust comparisons across laboratories, and with theoretical predictions. The dispersivity of a porous medium is defined as $l = \sigma^2/2\langle\zeta\rangle$, where σ^2 is the variance of an asymptotically Gaussian tracer displacement distribution and $\langle\zeta\rangle$ is the mean displacement. Longitudinal and transverse dispersivities $l_\parallel$ and $l_\perp$ need to be considered separately, and both depend on reduced velocity $\mathrm{Pe} = \bar{v}d/D_m$, where $\bar{v}$ is the mean flow velocity, d is the sphere diameter, and D_m is the tracers' diffusion coefficient. Saffman predicted [5,6] logarithmic growth of $l_\parallel(\mathrm{Pe})$ in a random network of identical capillaries, and his prediction maps onto pulsed field gradient nuclear magnetic resonance (PFG-NMR) results in RPMS [7] if one takes the capillaries to be about twice as long as they are wide. By contrast, the experimental transverse dispersivity $l_\perp(\mathrm{Pe})$ of a RPMS does not grow, it decreases monotonically with Pe and can be described by a model incorporating three pore scale mixing processes governed by diffusion and flow around neighboring packed spheres [8]. The velocity dependence of longitudinal and transverse dispersion is governed by diffusion perpendicular to the local flow. It couples flow zones to stagnation zones, which is important for longitudinal dispersion, and it couples streamlines at the center of a pore, which is important in transverse dispersion.

The RPMS with its known dispersion properties is a decidedly homogeneous random porous medium. The present work introduces short-range heterogeneity to the RPMS by incrementally adding small monodisperse spheres into the pore space. The resulting bidisperse packings exhibit partially plugged pore spaces analogous to those arising naturally in multiphase phase flows during oil production, where capillary forces may trap water in the formation, or analogous to pore spaces plugged by biofilms or filtrates [9], or to fouled separation columns and reactors, to name a few examples. Our homogeneous bidisperse packings retain the RPMS's fundamental conceptual simplicity, enabling comparison with simulations and theory. We show how findings for the bidisperse case connect with those of the RPMS [7,8,10].

A RPMS is characterized experimentally by two parameters, the sphere diameter d and packing porosity ϵ, or equivalently the sphere diameter and a reference length $\lambda = 6r_h$, where r_h is the volume-to-surface ratio $V_p/S_p = d/6 \times \epsilon/(1-\epsilon)$ of the pore space. In a bidisperse packing two additional parameters must be set based on presumed interest: (1) the ratio of sphere diameters d_L/d_s, where d_s and d_L are the diameters of small and large spheres, and (2) the relative number densities n and N for small and large spheres, respectively. In order to use small spheres as random obstructions in a macroscopically homogeneous random matrix of large spheres, we choose $d_L/d_s = 5$, a ratio for which a small sphere fits tightly into the smallest possible pore of the closest possible packing of large spheres, the tetrahedal void space in a fcc unit cell. To set n/N we take the number of pores, however defined, to be approximately equal to N. Six packings were prepared with ratios $n/N \in \{0, 1/3, 1, 3, 6, 9\}$ to span compositions from the dilute limit $n/N < 1$, where some pores are plugged but many are not, up to a presumed "overfilled" limit $n/N \gg 1$. The experiments with $n/N = 0$ serve as a reference for the five bidisperse packings with $n/N > 0$, and to verify that the current quantitative results are consistent with prior work on RPMS.

The porosity and dispersive properties of a RPMS, and by extension those of a bidisperse packing, depend on how the packing is made: experimental porosities range from $\epsilon \simeq 0.45$ of the random loose packing (RLP) down to random close packed (RCP) porosities $\epsilon_{\mathrm{RCP}} \simeq 0.364$. The lowest porosities are typically attained by tapping or vibrating a random packing to compact it, until no further compaction is observed [11,12]. The definition of random close packing is heuristic—what density can you reach if you tap the packing often enough—and related to the theoretical maximally jammed packing (MJP) with minimal porosity of $\epsilon_{\mathrm{MJP}} \approx 0.366$ [13,14]. Our target arrangement of particles was a maximally dense (MJP/RCP) macroscopically homogeneous random packing of large spheres, with increasing numbers of small spheres sprinkled randomly into interstitial sites. This required a packing process minimizing surface shear flows, which are known to produce size segregation in binary mixtures [15–17], and eliminating the shaking or tapping steps otherwise used to prepare RCP packings, which are known to cause size segregation in the Brazil-nut problem [18–21]. Below, we describe a hands-off packing procedure which met these requirements and produced consistent and what experimentally appear to be maximally dense random packings. We then present the NMR-derived measurements of packing properties confirming the sought-after consistency of the packings, followed by a discussion of dispersion results.

Our flow tube was made of borosilicate glass (Götek-Labortechnik) and had an inner diameter of 16 mm. It was closed at the bottom with a porous disk flow distributor, backed by a piston with a grooved face and with a central channel to feed in fluids. The unloaded and dry flow tube was positioned vertically and hooked up to a flow loop described in Ref. [10]. A small volume of water was injected into the tube from below, until the surface of the porous flow distributor was just covered by water. This ensured that the distributor and the first few layers of spheres in the loaded packing would be wetted before saturation.

Mixtures of particles were prepared for each n/N, beginning with 26 g (18 ml) of large borosilicate spheres ($d_L = 196 \pm 14$ μm) weighed and poured into a transparent plastic storage container. A batch of small borosilicate spheres ($d_s = 41 \pm 3$ μm), weighed to produce the desired ratio n/N to within 1%, were sprinkled on top of the larger ones. The container was closed and shaken vigorously to send the spheres flying about inside, for gaslike mixing of small and large spheres. The prepared mixture of particles n/N was poured into the prepared flow tube through the double-funnel setup sketched in with Fig. 1. The inner cone-shaped funnel was fashioned from filter paper. It rested within the outer plastic funnel. The tip of the inner funnel was cut off to make a small opening through which particles dumped into the paper funnel would drizzle downwards, like sand in an hour glass. After falling for some 4 cm, the thin stream of falling particles hit

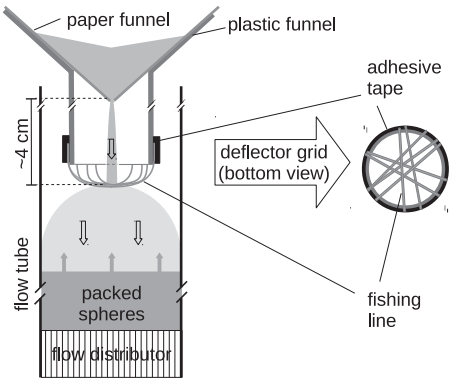

FIG. 1. Particle loading setup. The stream of falling particles is scattered by the deflector grid to produce spatially uniform deposition below.

a deflector grid made from short pieces of fishing line strung across the opening of the outer funnel, as shown in Fig. 1. Deposition times were on the order of minutes. The scattered stream deposited particles uniformly onto the porous packing growing from below, evinced by the fact that the packing surface rose and remained flat and horizontal throughout, in contrast to the cone formation and avalanches observed with sand piles in hour glasses. The absence of avalanches eliminated collective flows which might have otherwise led to size segregation. The loaded flow tube was saturated with water from below at a flow rate of 1 ml/h. Then the filled tube was closed up with another flow distributor assembly on top, and a few liters of water were circulated through it, at different rates, to check for fluid leaks and to verify that the size of the packing did not change with flow rate or time; it did not. The filled tube was then placed inside the vertical access magnetic resonance imaging (MRI) system manufactured by Aspect Imaging. MRI showed no evidence of trapped bubbles.

Displacement encoding PFG-NMR measurements were conducted on the central 2 cm of the packing (equidistant from inlet and outlet), employing a variant [22] of standard displacement encoding PFG-NMR sequences [23] in which the protons of water are the tracers. Water was pumped through the packing at constant volumetric flow rate $\dot{V}$ with a pair of piston pumps (ISCO) providing pulseless flow. Pulsed field gradients were applied in parallel or perpendicular to the mean flow direction to encode displacements in the longitudinal and transverse directions, respectively. The complex NMR signal is given by $S(q, \bar{v}, \Delta, D_m) = \langle e^{iq\zeta_j(\bar{v},\Delta,D_m)} \rangle$, where ζ_j is the displacement of a proton spin j in the direction of the displacement encoding pulsed field gradients. Δ is the evolution interval separating encoding and decoding PFG pulses, q is the amplitude of the displacement encoding wave vector set up by the PFG pulses, and D_m is the molecular diffusion coefficient of water. NMR signals were acquired for different flow rates and different values of Δ and q. A

self-consistent cumulant analysis [22] of a set $\{S(q_\parallel)\}$ yields the mean tracer displacement $\langle\zeta\rangle$, the corresponding mean flow velocity $\bar{v} = \langle\zeta\rangle/\Delta$, and the variance $\sigma_\parallel^2$ of tracer displacements along the direction of flow. The porosity is equal to $\epsilon = \dot{V}/A\bar{v}$, where $A = 2$ cm^2 is the cross section of the flow tube. As in RPMS, the distribution of mean flow velocities P_v in our bidisperse packings has finite width β and variance $\beta^2 = \langle(v-\bar{v})^2/\bar{v}^2\rangle$, due to wall effects [7]. As in RPMS, measured longitudinal dispersivities $l'_\parallel = \sigma_\parallel^2/2\langle\zeta\rangle$ grow linearly with mean displacements $l'_\parallel = l_\parallel(\mathrm{Pe}) + \langle\zeta\rangle\beta^2/2$. The intrinsic longitudinal dispersivity $l_\parallel(\mathrm{Pe})$ of the infinite bidisperse packing and the variance β^2 are determined from the slope and y intercept of measured $l'_\parallel$, as shown in the inset of Fig. 2(b). Note that absent wall effects these slopes and β would be zero, but in the laboratory it is inevitably finite and can be on the order a few percent. Separate measurements perpendicular to the flow yield the variance $\sigma_\perp^2$ of transverse displacements. The velocity-dependent transverse dispersivity is $l_\perp(\mathrm{Pe}) = \sigma_\perp^2/2\langle\zeta\rangle$, averaged over multiple evolution times at the same fixed velocity. Of the four measured quantities, porosity ϵ and variance β^2 are velocity independent and probe the consistency of the packing procedure from one packing to the next. The other two quantities, $l_\parallel(\mathrm{Pe})$ and $l_\perp(\mathrm{Pe})$, quantify the intrinsic velocity-dependent dispersivities, the pore scale transport quantities amenable to simulation in infinite packings implemented with periodic boundary conditions, or to theory with models including obstructions or distributed channel sizes.

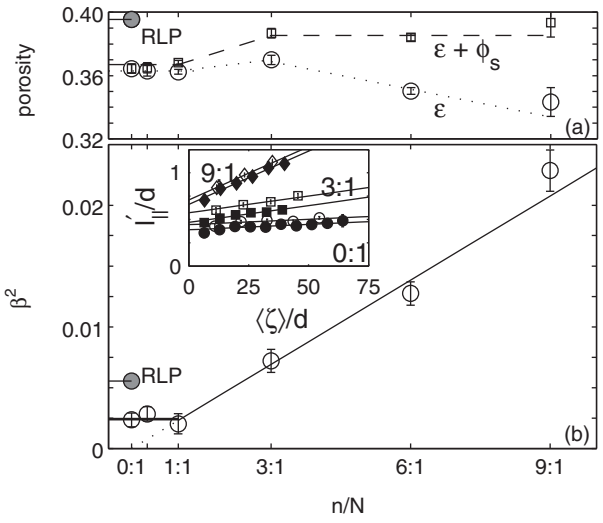

FIG. 2. All lines are a guide to the eye. (a) The porosity (o) $\epsilon = 0.363$ of packings $n/N \leq 1$ is consistent with RCP/MJP packing $\epsilon_{\mathrm{MJP}} = 0.366$. Small spheres wedge large spheres apart above $n/N = 1$, as discussed in text. (b) The variance β^2 of the distribution of normalized drift velocities [7] depends on the concentration of small spheres for $n/N \geq 1$, indicating shift of flux between wall zone and bulk of the packing.

Measured porosities of all packings are shown with open circles in Fig. 2(a). They fall into a range from 0.34 to 0.37; the loose packing labeled RLP (E2 of Ref. [10]) is shown with a filled circle. In packings $n/N \leq 1$, less than 1% of the packing volume is occupied by small spheres. These packings exhibit consistent and near equal porosities with a mean value of $\bar{\epsilon} = 0.3633(11) \approx \epsilon_{\mathrm{RCP}}$. The error bars on the order of 1% reflect scatter in the porosity measurement; the common systematic accuracy set by the calibration of the NMR equipment is on the order of 1% as well. The approximate equality of porosities for $n/N \leq 1$ confirms that the filling procedure described above is consistent and produces approximately RCP packings, close to maximally jammed RPMS state with $\epsilon_{\mathrm{MJP}} = 0.366$. The remaining three packings $n/N \geq 3$ exhibit decreasing porosities with increasing n/N, down to $\epsilon_{\mathrm{min}} = 0.34$ for $n/N = 9$, consistent with small spheres filling vacant pores in the pore space. Notably, however, the packing $n/N = 3$ exhibits a larger porosity than packings $n/N \leq 1$. This incongruity—a rise in porosity as the number of small spheres is increased—can be understood once we consider the sum of porosity and volume fraction ϕ_s occupied by small spheres, plotted with open squares in Fig. 2(a). This sum, and with it the volume fraction $\phi_L = 1 - (\epsilon + \phi_s)$ occupied by large spheres, is approximately constant for the three packings $n/N \geq 3$, with $\epsilon + \phi_s = 0.388(5)$. This suggests that for $n/N \approx 1$ all available pores in the RCP are all filled and that additional small spheres must wedge apart the arrangement of large spheres to occupy $\phi_L \approx 0.612(5)$. The "wedged open" pore space then gradually fills up as more small spheres are added, $n/N \to 9$. In what follows we shall see that the other measurements support the conjectured existence of two distinct random structures, one a partially plugged RCP packing of large spheres, and the other an arrangement of large spheres wedged apart by the smaller ones.

The variance β^2 of P_v shown in Fig. 2(b) is a measure of macroscopic flow homogeneity in a packing. It is derived from the slope of $l'_\parallel$ vs $\langle\zeta\rangle$ shown for three representative packings and two velocities each in the inset of Fig. 2(b). For $n/N \in \{0, 1/3, 1\}$ the value of β^2 is constant, which means that there is no measurable shift of flux between the wall zone and the bulk of the packing upon addition of small spheres; the width of the distribution of normalized velocities P_v is $\beta \approx 5\%$. This width triples to $\beta = 15\%$ for $n/N = 9$, and the plot shows the variance β^2 rising approximately linearly with n/N. This is consistent with a systematic redistribution of flux between the bulk and the boundary zone near the tube wall for $n/N \geq 3$.

With porosity ϵ and variance β^2 indicating the existence of two distinct types of disorder for $n/N \leq 1$ and $n/N \geq 3$, we now consider the intrinsic dispersivities of our bidisperse packings. Figure 3(a) shows $l_\parallel(\mathrm{Pe})/r_L$ for all packings, where r_L is the radius of a large sphere. Figure 3(b) shows the corresponding transverse dispersivities $l_\perp(\mathrm{Pe})/r_L$. The

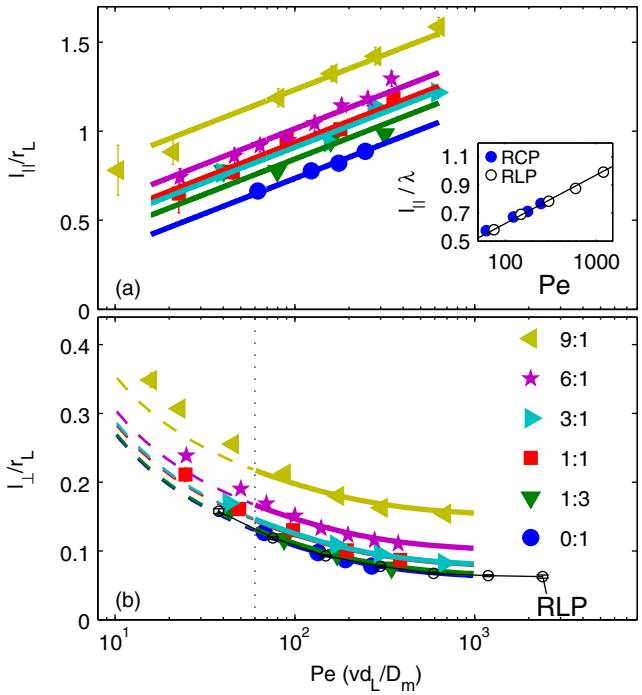

FIG. 3. (a) The Pe-dependent $l_{\|}/r_L$ shows equal logarithmic growth for all packings n/N, offset by increased mechanical dispersion as $n/N \to 9$. Inset: The $n/N = 0$ data and RLP data $l_{\|}/\lambda$ coincide [10]. (b) For Pe$\gtrapprox$60, added mechanical dispersivity shifts curves of $l_{\perp}/r_L$ versus Pe up, as $n/N \to 9$. The earlier RLP results (open circles) coincide with the present $n/N = 0$ data.

solid lines in both represent the known velocity-dependent dispersivities of RPMS—logarithmic growth for the $l_{\|}$, and the decreasing $l_{\perp}$ of Ref. [8]—now shifted vertically by fitted offsets parametrizing added mechanical dispersion. For the transverse case, we consider data for Pe $\gtrsim 60$ only, velocities where mechanical and diffusively coupled mechanical dispersion dominate the transverse dispersion process. This figure illustrates that, to leading order, increasing amounts of small spheres add systematic velocity-independent (mechanical) dispersivity to the known longitudinal and transverse dispersivity of the RPMS, even in the regime $n/N \leq 1$ where neither porosity nor β^2 show variation with n/N.

Finally, Fig. 4 quantifies the systematic added longitudinal and transverse dispersivity, i.e., the respective differences between the fitted lines of Fig. 3 and the reference curve $n/N = 0$, with standard error bars. Between $n/N = 0$ and $n/N = 1$ longitudinal dispersivity rises by up to $\delta l_{\|} \approx 0.2 r_L$, which represents a significant increase on longitudinal dispersivities of monodisperse packings, for the velocities Pe > 10 of Fig. 3. The transverse dispersivity also rises, by $\delta l_{\perp} \approx 0.017 r_L$ for $n/N = 1$. This again is a significant rise, compared to the intrinsic mechanical dispersivity of a RPMS, which is $l_m \approx 0.06 r_L$. Surprisingly, tripling the concentration of small spheres from $n/N = 1$ to $n/N = 3$ causes longitudinal and

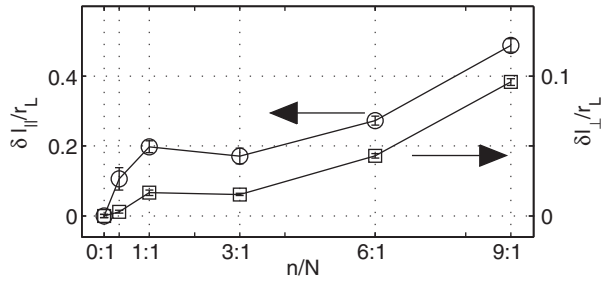

FIG. 4. Mechanical mixing offsets from the $n/N = 0$ data, taken from the fitted lines in Fig. 3.

transverse dispersivities to plateau or even decrease, to within the uncertainty of the measurement. This means that the added small spheres actually improve the macroscopic homogeneity of the flow field in this concentration range, a finding which might inform the design of robust packings for filtration applications, though there is of course a difference between obstructions added in the packing process and those arising by filtration. Beyond $n/N = 3$ dispersivities rise again, albeit more slowly than before. Notably the dispersivities and their unexpected dependence on the density of small spheres also point to two distinct dispersion regimes, one for $n/N \leq 1$ and another for $n/N \geq 3$, separated by a transition plateau. This distinct concentration dependence of $\delta l_{\|}$ and $\delta l_{\perp}$ is consistent with the distinct random packing arrangement conjectured in the discussion of ϵ and β^2. Now this identification of qualitatively distinct behaviors is derived from intrinsic dispersion properties. It should also be noted that the added mechanical dispersivity is anisotropic with $\delta l_{\|}/\delta l_{\perp} \gtrsim 3$ for the "wedged open" arrangements ($n/N \geq 3$), and larger still for the dilute packing ($n/N = 1/3$) where the transverse dispersion changes much less than the longitudinal dispersivity does. This may indicate small overlap of flow disturbances around plugged pores, in the dilute regime.

In conclusion, this Letter determines the intrinsic dispersivity of a class of bidisperse packings with $d_L/d_s = 5$, in the limit where most of the solid matrix is occupied by the larger spheres. There is evidence for two distinct types of random arrangements in packings of spheres, above and below relative sphere density $n/N = 1$. The packings' longitudinal and transverse dispersivities—in the advection dominated regime Pe > 60 for $l_{\perp}$ and down to lower velocities for the longitudinal $l_{\|}$—is approximately equal to that of a RPMS made of large spheres alone, plus some concentration-dependent, non-negligible, and anisotropic mechanical mixing in the longitudinal and transverse directions.

*uscheven@umich.edu

[1] E. Perfect, M. C. Sukop, and G. R. Haszler, Prediction of dispersivity for undisturbed soil columns from water retention parameters, Soil Sci. Soc. Am. J. **66**, 696 (2002).

[2] D. Schulze-Makuch, Longitudinal dispersivity data and implications for scaling behavior, Ground Water **43**, 443 (2005).
[3] E. Charlaix, J. P. Hulin, and T. Plona, Experimental study of tracer dispersion in sintered glass porous materials of variable compaction, Phys. Fluids **30**, 1690 (1987).
[4] M. Kaviany, *Principles of Heat Transfer in Porous Media*, 2nd. ed. (Spinger-Verlag, New York, 1995).
[5] P. G. Saffman, A theory of dispersion in a porous medium, J. Fluid Mech. **6**, 321 (1959).
[6] P. G. Saffman, Dispersion due to molecular diffusion and macroscopic mixing in flow through a network of capillaries, J. Fluid Mech. **7**, 194 (1960).
[7] U. M. Scheven, R. Harris, and M. L. Johns, Intrinsic Dispersivity of Randomly Packed Monodisperse Spheres, Phys. Rev. Lett. **99**, 054502 (2007).
[8] U. M. Scheven, Pore-Scale Mixing and Transverse Dispersivity of Randomly Packed Monodisperse Spheres, Phys. Rev. Lett. **110**, 214504 (2013).
[9] J. D. Seymour, J. P. Gage, S. L. Codd, and R. Gerlach, Anomalous Fluid Transport in Porous Media Induced by Biofilm Growth, Phys. Rev. Lett. **93**, 198103 (2004).
[10] U. M. Scheven, S. Khirevich, A. Daneyko, and U. Tallarek, Longitudinal and transverse dispersion in flow through random packings of spheres: A quantitative comparison of experiments, simulations, and models, Phys. Rev. E **89**, 053023 (2014).
[11] G. D. Scott and D. M. Kilgour, The density of random close packing of spheres, Br. J. Appl. Phys., J. Phys. D **2**, 863 (1969).
[12] R. D. Kamien and A. J. Liu, Why is Random Close Packing Reproducible?, Phys. Rev. Lett. **99**, 155501 (2007).
[13] S. Torquato, T. M. Truskett, and P. G. Debenedetti, Is Random Close Packing of Spheres Well Defined?, Phys. Rev. Lett. **84**, 2064 (2000).
[14] C. Song, P. Wang, and H. A. Makse, A phase diagram for jammed matter, Nature (London) **453**, 629 (2008).
[15] H. A. Makse, S. Havlin, P. R. King, and H. E. Stanley, Spontaneous stratification in granular mixtures, Nature (London) **386**, 379 (1997).
[16] J. M. Ottino and D. V. Khakar, Mixing and segregation of granular materials, Annu. Rev. Fluid Mech. **32**, 55 (2000).
[17] H. A. Makse, Grain segregation mechanism in aeolian sand ripples, Eur. Phys. J. E **1**, 127 (2000).
[18] A. Rosato, K. J. Strandburg, F. Prinz, and R. H. Swendsen, Why the Brazil nuts are on Top: Size Segregation of Particulate Matter by Shaking, Phys. Rev. Lett. **58**, 1038 (1987).
[19] J. B. Knight, H. M. Jaeger, and S. R. Nagel, Vibration-Induced Size Separation in Granular Media: The Convection Connection, Phys. Rev. Lett. **70**, 3728 (1993).
[20] M. E. Mobius, B. E. Lauderdale, S. R. Nagel, and H. M. Jaeger, Brazil-nut effect: Size separation of granular particles, Nature (London) **414**, 270 (2001).
[21] J. M. N. T. Gray and A. R. T Hornton, A theory for particle size segregation in shallow granular free-surface flows, Proc. R. Soc. A **461**, 1447 (2005).
[22] U. M. Scheven, Constant gradient PFG sequence and automated cumulant analysis for quantifying dispersion in flow through porous media, J. Magn. Reson. **237**, 152 (2013).
[23] R. M. Cotts, M. J. R. Hoch, T. Sun, and J. T. Markert, Pulsed field gradient stimulated echo methods for improved NMR diffusion measurements in heterogeneous systems, J. Magn. Reson. **83**, 252 (1989).